Hindawi
Advances in Polymer Technology
Volume 2023, Article ID 4319998, 15 pages
https://doi.org/10.1155/2023/4319998

Research Article

The Synergy of Nanosilica and Zinc Diethyl Hypophosphite Influences the Flame Retardancy and Foaming Performance of Poly(Ethylene Terephthalate)

Jiaxin Zheng,[1] **Congxiao Wang**,[1] **Yuyin Zhao**,[1] **Menghao Guo**,[1] **Yadong He**,[1,2] **and Chunling Xin**[1,2]

[1]*College of Mechanical and Electrical Engineering, Beijing University of Chemical Technology, Beijing 100029, China*
[2]*Engineering Research Center for Polymer Processing Equipment, Ministry of Education, Beijing 100029, China*

Correspondence should be addressed to Chunling Xin; xincl@mail.buct.edu.cn

Received 13 September 2022; Revised 23 March 2023; Accepted 30 March 2023; Published 28 April 2023

Academic Editor: Kinga Pielichowska

In order to improve the flame retardancy of poly(ethylene terephthalate) (PET) and maintain its excellent foamability, nanosilica (nano-SiO_2), and zinc diethyl hypophosphite (ZDP) were selected as synergistic flame retardants, and pyromellitic dianhydride (PMDA) was used as a chain extender to carry out flame retardant and chain extension modification of PET simultaneously. The flame retardancy and flame-retardant mechanism of modified PET were characterized by limiting oxygen index, vertical combustion test, thermogravimetric analysis, and SEM. Dynamic rheological test and DSC were used to analyze the rheological and thermal properties. The foaming ability was also studied by batch foaming experiments. The test results indicated that nano-SiO_2 and ZDP had a synergistic effect, which could significantly improve flame retardancy of PET. The vertical combustible grade of modified PET reached V-0 grade, and the limiting oxygen index increased from 21% to about 30%. The role of nano-SiO_2 on the flame retardancy of PET was mainly to increase compactness and strength of the carbon layer, which could block combustible gas produced by the pyrolysis of PET and resist dripping behavior. At the same time, the addition of nano-SiO_2 increased the crystallization temperature and crystallinity of PET. Otherwise, nano-SiO_2 could act as a bubble-nucleating agent and improve the foaming ability of modified PET. When the addition amount was 1 wt%, not only did the maximum foaming ratio increase but the foaming temperature zone was also widened from 225°C-235°C to 225°C-250°C. Finally, a flame-retardant PET system with good foaming property was proposed.

1. Introduction

Poly(ethylene terephthalate) (PET) foam has been widely used in power blades, electronic packaging, solid-state lighting reflective material, and other fields [1–3], due to its excellent mechanical properties, high temperature dimensional stability, good chemical resistance, and recyclability. With the development of PET foaming technology, PET foam with more density specifications has been developed. As a result, PET foam has widespread application in construction, automobiles, and other fields, which require higher flame retardancy. However, due to its low charring capacity, the limiting oxygen index of PET is only 21%. And it is easy to drip and cause secondary combustion during a fire. Many flame retardants and processing technologies suitable for PET have been proposed [4–7].

Flame retardants used in PET can be divided into two kinds: additive and reactive. Reactive flame retardants are copolymerized with terephthalic acid and glycol, and flame-retardant elements are embedded into the molecular chain through polymerization. Therefore, they have little impact on the mechanical properties of PET, and the flame retardant molecules are not easily precipitated [8]. Nevertheless, reactive flame-retardant polyester is difficult

to synthesize, resulting in poor economics [9]. Moreover, flame retardant polyester has low reactive activity, making it difficult to improve viscoelastic properties through melt chain extension [10]. However, high viscoelasticity is the decisive factor that affects the success of foaming. Additive flame retardants are directly blended with PET at high temperature. This method is simple, fast, and cheap. However, blending flame retardants has a great impact on the mechanical properties of PET, which also reduces the melt strength and foaming properties [11].

Halogen flame retardants have excellent flame retardancy, but their combustion products such as dioxins will accumulate in the environment and eventually be absorbed or ingested by humans and animals. These products can produce great harm to the human body and environment [12], so they have been gradually abandoned around the world [13]. Relatively speaking, flame retardants containing phosphorus also have high flame-retardant efficiency. Groups containing phosphorus will decompose during the combustion to form phosphoric acid or anhydride during combustion, which can act as a dehydrating agent of the polymer. Phosphoric acid draws H_2O from PET and stimulates formation of char. At the same time, phosphorus flame retardants also have a certain effect on reducing melt viscosity, so they can take away a large amount of heat released during combustion through melt dripping [14]. Melt dripping is beneficial to the self-extinguishing of PET, but it will be easier to cause secondary combustion. In order to suppress this effect, Zhao and Wang [5] copolymerized the ionomer monomer SHPPP/DHPPO-Na onto the PET chain. They hoped to improve the melt viscosity of PET through physical cross-linking network formed by ion aggregation. Nevertheless, the disadvantage of the copolymer was a reduction of crystallinity, which would decrease the mechanical properties and heat resistance of PET.

Zinc diethyl hypophosphite (ZDP), which melts at about 220°C, can be blended with PET at high temperature. Therefore, ZDP can disperse well and has excellent compatibility with PET [15]. Salaun et al. [16] selected Exolit OP950 and nanosilica particles to improve the flame retardancy of PET textiles. They found that pkHRR was reduced significantly when Exolit OP950 was added alone, but it would promote the release of smoke from the polymer, which might cause potential risks for people in a fire [17]. Its flame retardant efficiency was not satisfactory, and it could not suppress the melting dripping phenomenon, even if the load reached 20 wt%. Nanosilica had synergy with Exolit OP950 on flame retardancy, which could improve the viscosity of PET textiles at high temperature to suppress melt dripping. Additionally, it could also have an effect on smoke suppression.

Many studies have shown that nano-fillers can play a role in flame retardant science as a synergist of phosphorus flame retardants [18, 19]. Nizar et al. [4] added POSS with different chemical structures to zinc phosphate to improve the flame retardancy of PET. They found that POSS can effectively reduce HRR and form a denser carbon layer structure. Wang et al. [20] measured the activation energy of the thermal oxidative degradation of PET/MMT nanocomposites by Kissinger and Flynn-Wall-Ozawa methods. They believed there was a higher activation energy after adding nano-MMT.

Nano-SiO_2 also has a certain effect on the flame retardancy of polymer materials. Zheng et al. [21] found that the addition of nano-SiO_2 increased the thermal decomposition activation energy of PET when the mass loss was 0-20 wt% by analyzing the thermal decomposition kinetics of PET/nano-SiO_2 nanocomposites. The results indicated that nano-SiO_2 could improve the thermal stability of PET very well. Gao et al. [22] used nano-SiO_2 and an intumescent flame retardant to improve the flame retardancy of epoxy resin. By observing SEM images, they found that carbon layer of EP/IFR was fragile and fragmentary without nano-SiO_2, which could not protect the underlying material from fire. The carbon layer was more solid after adding nano-SiO_2. Besides, it became continuous and compact, which could prevent combustible gas from coming into contact with fire.

Nano-SiO_2 can also be used as a nucleating agent for PET to improve the foaming performance of PET. Xu [23] found that nano-SiO_2 could affect growth of cells by improving the viscoelasticity of PS. It could also be used as a nucleating agent to improve cell density of PS. Wang et al. [9] studied the effect of nanoclay on supercritical CO_2-foamed polypropylene and found that it increased the cell density of the composites. When the content of nanoclay was high, it also increased the tensile melt strength and shear complex viscosity of PP.

In this study, an environmentally friendly phosphorus flame retardant, diethylzinc hypophosphite (ZDP) was selected as the main flame retardant. Its good compatibility with PET could reduce the damage of melting viscoelasticity and mechanical properties. In order to increase the flame-retardant efficiency of ZDP and inhibit dripping during a fire, nano-SiO_2 was added as a synergist to improve thermal stability of PET/ZDP composites and the compactness of the charred layer. Meanwhile, the ZDP/SiO_2 synergistic flame-retardant mechanism was analyzed through thermogravimetric tests and micromorphology analysis of the residual carbon layer. Additionally, the influence of SiO_2 on the foaming performance of flame-retardant PET was analyzed by dynamic rheological testing and DSC.

2. Experiment

2.1. Materials. Poly (ethylene terephthalate) (PET) used in this study was provided by Sinopec Yizheng Chemical Fiber Co., Ltd. Its intrinsic viscosity was 0.8 dl/g. ZDP, used as flame retardant, was bought from Qingdao Opry New Material Co., Ltd. Its phosphorus mass fraction was 19.5%-21.0 wt%. The type of nano-SiO_2 was SWHT-107, purchased from Beijing Siweihaote New Material Technology Co., Ltd. Its particle size is 50-300 nm, and the surface is treated with hydrophobic groups. Pyromellitic dianhydride (PMDA) was supplied by Aladdin Reagent (Shanghai) Co., Ltd.

2.2. Reactive Blending. The process of reaction between PMDA and PET/ZDP/nano-SiO_2 composites could be

detected by the HAAKE Polylab OS, which could record the variation of torque versus time. The processing conditions were 270°C and 60 rpm. All virgin materials should be dried at 120°C for 12 h in vacuum oven before blending. The samples obtained from Haake Polylab OS would be used to carry out thermogravimetric analysis, rheological characterization, DSC, and batch foaming processes.

Reactive extrusion processing and injection molding were used to obtain standard samples for combustible performance tests. They were carried out using a twin-screw extruder (ZSK25-WLE type), manufactured by W&P Company, and injection molding machine (HTF120X2 type), provided by Haitian Group Co., Ltd. The temperature of each part of the extruder was 200°C, 245°C, 250°C, 255°C, 260°C, 265°C, 265°C, 265°C, and 265°C, respectively. And a screw speed of 100 rpm was used. The injection molding machine had 5 parts for adjusting temperature, set at 240°C, 250°C, 265°C, 265°C, and 250°C, respectively.

The formula has been listed in Table 1.

Table 1: Formula.

Sample	PET	ZDP	Nano-SiO_2	PMDA	Antioxidant 1010
10Z	90%	10%	0%	0.6%	0.1%
10Z/1S	89%	10%	1%	0.6%	0.1%
10Z/3S	87%	10%	3%	0.6%	0.1%
10Z/5S	85%	10%	5%	0.6%	0.1%

Table 2: limiting oxygen index and vertical combustion test of Pet/Zdp/nano-Sio_2 composites.

Materials	LOI/%	$t_1 + t_2$/s	Dripping	UL94
Pure PET	21.6	≥30	Yes	NR
10Z	28.5	5.95	Yes	V-2
10Z/1S	29.3	5.125	Yes	V-2
10Z/3S	29.1	6.53	Yes	V-2
110Z/5S	30.9	2.72	No	V-0

2.3. Characterization of Samples. Dynamic rheological testing, The Haake Mars III rheometer (Thermo Fisher Scientific, USA) was used to measure shear rheological properties. The samples, which were dried at 120°C in vacuum oven for 12 hours, were placed on steel parallel plate that was heated to 270°C. The samples were then pressed into a 1 mm thickness in an inert environment, and the frequency sweeps changed from 100 to 0.1 rad/s after starting

Thermogravimetric analysis. Samples weighing about 10 mg were placed in an alumina crucible. A thermogravimetric analyzer (ZCT-B type), manufactured by Beijing Jingyi Hi-Tech Instrument Co., Ltd., recorded the quantity variation as the temperature rose from 100°C to 800°C in an inert environment or oxidation conditions. The curve of DTA, which represents the heat flow variation, was drawn at the same time. The differential curve of TG would be obtained through the analysis software

Differential scanning calorimetry. The differential scanning calorimeter (Q2000) was manufactured by TA Instrument in America. Samples weighing about 6-8 mg were put into the aluminum crucible. The test would be carried out in an inert environment and proceeded as follows: First, the temperature was rapidly raised to 300°C and maintained for 3 min. Then, it was lowered to 30°C at a speed of 10°C/min and maintained for 3 min. Finally, the temperature was raised to 300°C again at a speed of 10°C/min.

Vertical combustion and the limiting oxygen index test. The standard size of the splines for vertical combustion was 125 × 13 × 3.2 mm. The combustible time and whether the cotton was ignited by dripping were recorded. The standard size of the splines for LOI testing was 80 × 10 × 4 mm. The oxygen content was continuously adjusted to find a suitable ratio to sustain the samples to burn steadily. The vertical combustion test followed the standard GB/T 2408—2021, while limiting oxygen index test followed the standard GB/T 2406.2—2009

Scanning electron microscopy. Samples of the carbon layer should be treated with gold sputtering. As for foams, they should be cut to expose their cross-section before gold sputtering. Then the samples will be observed under scanning electron microscopy (TM4000), which was manufactured by Hitachi, Japan.

Batch foaming experiment. Foaming experiments were performed in a high-pressure vessel using a procedure that simulated extrusion foaming techniques, as follows: The sample was placed into an autoclave (self-made) that was heated to 280°C, then filled with CO_2 until the pressure reached 15 MPa, and maintained for 20 min. Then, the autoclave was cooled to the foaming temperature and kept for 40 min, and the pressure was finally relieved quickly.

Determination of foaming ratio. A sponge densitometer (PMMD-A, Guance Test Instrument Co., Ltd, Beijing) was used to determine the density of samples before and after foaming, and the foaming ratio could be calculated according to

$$\text{Foaming ratio} = \frac{\rho_1}{\rho_2}. \quad (1)$$

ρ_1 is the density of sample before foaming, and ρ_2 is the density of sample after foaming.

3. Results and Discussion

3.1. Flame Retardant Performance

3.1.1. Effect of Nano-SiO_2 as Synergist of ZDP on Flame Retardance of PET. LOI and vertical combustion test were used to estimate the flame retardancy of modified PET with different contents of nano-SiO_2. The results are shown in Table 2. It was found that the addition of ZDP improved the LOI of PET from 21% to 28.5%, which indicated that PET had changed from a flammable material to a refractory material. However, the melt-dripping phenomenon still existed. The LOI of PET increased with the addition of nano-SiO_2. When the amount was 5 wt%, LOI reached 30.9% and the vertical combustion grade also reached the V-0 level due to the inhibition of melt dripping by nano-

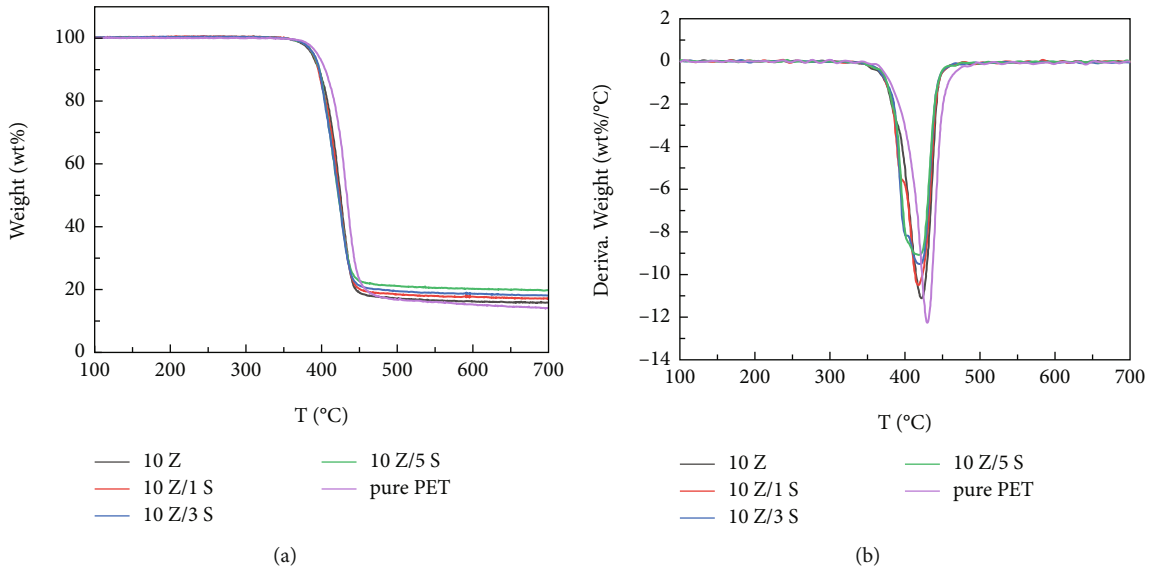

Figure 1: The thermal weight loss curve of modified PET in N_2 atmosphere (a) TG curve. (b) DTG curve.

SiO_2. However, nano-SiO_2 did not have a significant effect at low concentrations. Regarding the reduction in LOI with a load of 3 wt% nano-SiO_2, this may be because nanoparticles agglomerate in the PET matrix and form aggregates. Meanwhile, the PET matrix flows along the particle aggregates to the heat source after being heated and melted and decomposes to provide fuel for the combustion reaction at high temperatures, leading to the formation of the "wick effect" [24, 25]. As for the increase in LOI after adding 5 wt% nano-SiO_2, its the result of the competition between the improvement of thermal stability by nano-SiO_2 and the enhancement of carbon layer quality after combustion and the "wick effect." Moreover, the thermal decomposition kinetics analysis in Section 3.1.3 supports this conclusion. The activation energy decreased when the load of nano-SiO_2 was 3 wt% and increased again when the load was 5 wt%.

3.1.2. Thermogravimetric Analysis. Flame retardancy of polymer is directly related to the thermal decomposition step [22], so the thermogravimetric behavior can be used to analyze the mechanism of combustion. Thermal oxidative degradation occurs on the surface of the polymer during ignition with the participation of air. A stable fire can prevent air from getting in touch with the polymer after ignition, so pyrolysis in the condensed phase is essentially anaerobic at this stage. In order to further reveal the flame-retardant mechanism, it is necessary to study and compare the thermal decomposition behavior of modified PET in air and nitrogen.

Thermogravimetric curves of modified PET in an N_2 atmosphere are shown in Figure 1, and the detailed characteristic data are listed in Table 3. It could be found that the initial decomposition temperature $T_{5\%}$ of PET reduced to 387°C from 395°C after adding 10 wt% ZDP. The reason was that phosphoric acid, pyrophosphoric acid, and other substances that could strengthen the dehydration and charring of PET

Table 3: Characteristic data of modified PET Tg in N_2 Atmosphere.

Sample	$T_{5\%}$/°C	$T_{50\%}$/°C	C_{600}/%	T_{max}/%	$b_{1/2}$/°C
Pure PET	395	434	15.53	431	28.7
10Z	387	425	16.25	422	34.8
10Z/1S	389	423	17.69	418	42.8
10Z/3S	390	423	18.68	420	42.1
10Z/5S	389	423	20.25	419	40.9

to promote the formation of the carbon layer [26] are formed by the decomposition of phosphate flame retardants at high temperature. On the contrary, the addition of nano-SiO_2 could increase $T_{5\%}$, implying that nano-SiO_2 could improve the thermal stability of PET/ZDP composites.

With the increase in nano-SiO_2 content, thermal decomposition rate peak of the samples widened (Figure 2(b)), indicating that the maximum thermal decomposition rate of PET reduced. The half-peak width $b_{1/2}$ of each sample was calculated for comparison (Table 2). $b_{1/2}$ of pure PET is only 28.7°C. After adding 10 wt% ZDP, it increased to 34.8°C. There was an additional raise of $b_{1/2}$ when 1 wt% nano-SiO_2 was added in PET/ZDP blends. Nevertheless, if the content of nano-SiO_2 continued to increase, $b_{1/2}$ would no longer be affected. These changes revealed that ZDP and nano-SiO_2 could delay the thermal decomposition of PET.

Thermogravimetric curves of modified PET in an air atmosphere are shown in Figure 2, and the detailed characteristic data are listed in Table 4. There were two stages in the thermal oxidative degradation of the air. The first stage represented the thermal oxygen decomposition of the PET matrix and the formation of char. The second stage was the oxidation of residual carbon. The first peak of modified PET at 400-450°C decreased after adding ZDP and nano-SiO_2. The rise of T_{max2} with nano-SiO_2 content showed that nano-SiO_2 could improve the thermal oxygen stability of the

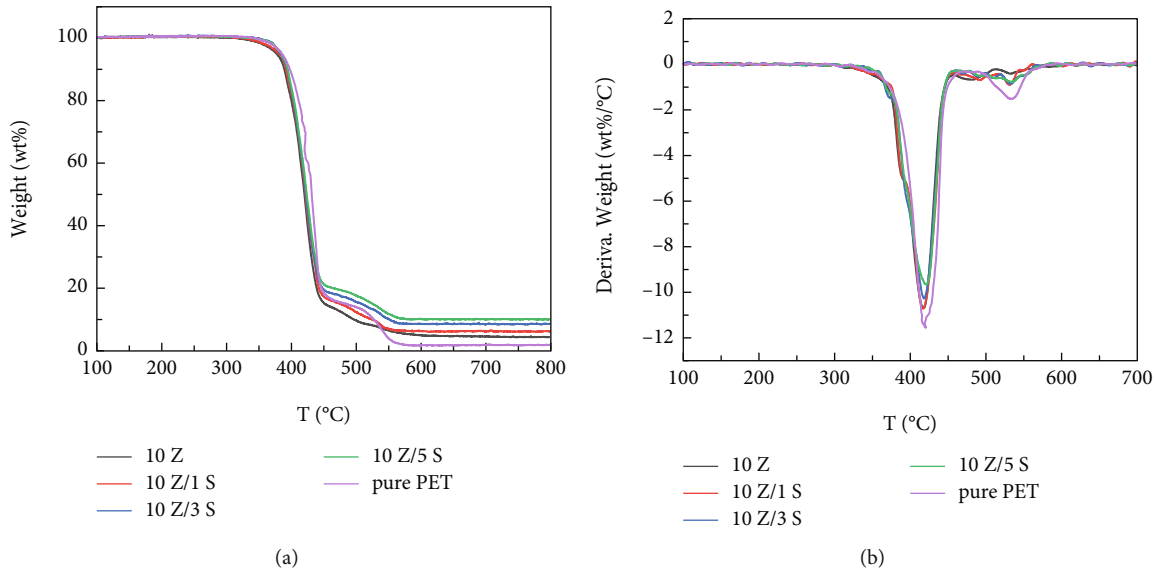

Figure 2: Thermal weight loss curve of adding nano-Sio_2 with different content in air environment. (a) TG curve. (b) DTG curve.

Table 4: TG analysis data of each sample in air atmosphere.

	$T_{5\%}$	$T_{50\%}$	T_{max1}	T_{max2}	C_{600}
Pure PET	385	431	420	532	1.70
10Z	377	419	418	533	4. 99
10Z/1S	380	421	417	532	6. 27
10Z/3S	383	422	418	533	8. 59
10Z/5S	384	423	421	535	10. 13

carbon layer. In the second thermogravimetric stage, the residual mass of pure PET decreased rapidly in a narrow temperature range, while the thermooxidative decomposition temperature range was significantly widened after adding ZDP and nano-SiO_2.

The residual mass difference curves (ΔTG) could be obtained by subtracting the TG curve of the 10Z sample from the TG curves of nano-SiO_2 samples with different contents (Figure 3). These curves are used to analyze the impact of nano-SiO_2 on the residual mass and thermal decomposition rate of PET in comparison to the 10Z samples.

There were two peaks in the ΔTG curves in the N_2 atmosphere (Figure 3(a)). There was a convex peak at about 400°C. At this temperature, ΔTG is greater than 0, which indicated that the residual mass of samples after adding nano-SiO_2 was higher than that of the 10Z sample. This also reveals that nano-SiO_2 can improve the thermal stability of PET/ZDP composites at the initial decomposition stage. ΔTG decreased rapidly between 390°C and 420°C, which indicated that nano-SiO_2 made PET decompose at a faster thermal decomposition rate after starting decomposition. And ΔTG had a significant rise after 420°C, corresponding to T_{max} in the N_2 environment. The reason might be that nano-SiO_2 did not volatilize and could remain in the carbon layer. It would cover the surface of the char to lower the thermal decomposition of PET.

The ΔTG curves in the air atmosphere illustrated in Figure 3(b) had a completely different trend from those in the N_2 atmosphere. It was always above the zero line, representing that nano-SiO_2 had a better promoting effect on the formation of the carbon layer in the air environment. ΔTG curves appeared with multiple peaks from the beginning of decomposition to 600°C, showing that nano-SiO_2 had different effects on the thermooxidative decomposition of PET in various temperature ranges. The rise after 550°C indicated the thermal decomposition rate of samples with nano-SiO_2 was lower than that of the 10Z sample. At the same temperature, the carbon layer had started thermal oxidation, meaning that nano-SiO_2 reduced the thermal decomposition rate of the carbon layer and improved its thermal stability.

3.1.3. Thermal Decomposition Kinetics. The flammability of PET is related to its thermal degradation behavior at high temperature. ZDP and nano-SiO_2, as flame retardants, will change the pyrolysis process of polymers. In order to understand the impact of ZDP and nano-SiO_2 on PET, the differential isoconversional method is used to determine the impact of thermal decomposition kinetics. This method can determine the thermal degradation stability of different products without knowing the specific reaction model. The model of the differential isoconversional method is shown in equation (2) [27]. And it can also be used to determine whether the single-step kinetic assumption is correct.

$$\ln\left(\beta_i\left(\frac{d\alpha}{dT}\right)_{\alpha,i}\right) = \ln\left[f(\alpha)A_\alpha\right] - \frac{E_\alpha}{RT_{\propto,i}}. \quad (2)$$

The activition energy (E_α) of each conversional rate (α) is determined by the slopes of $\ln\left(\beta_i(d\alpha/dT)_{\alpha,i}\right)$ vs. $1/T_{\propto,i}$. i represents the heating rate under linear heating conditions. R is the gas constant ($R = 8.314\,\mathrm{J\cdot mol^{-1}\cdot K^{-1}}$), and T is the temperature (unit is K). $\ln\left[f(\alpha)A_\alpha\right]$ is the reaction model,

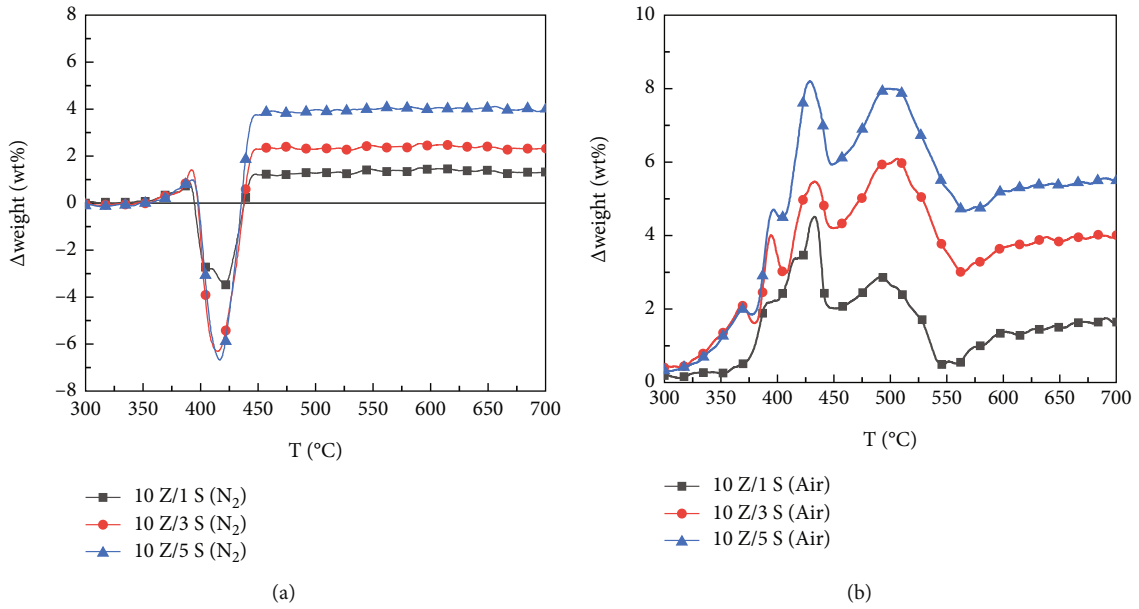

Figure 3: Residual mass difference curve (Δtg). (a) N_2 atmosphere. (b) Air atmosphere.

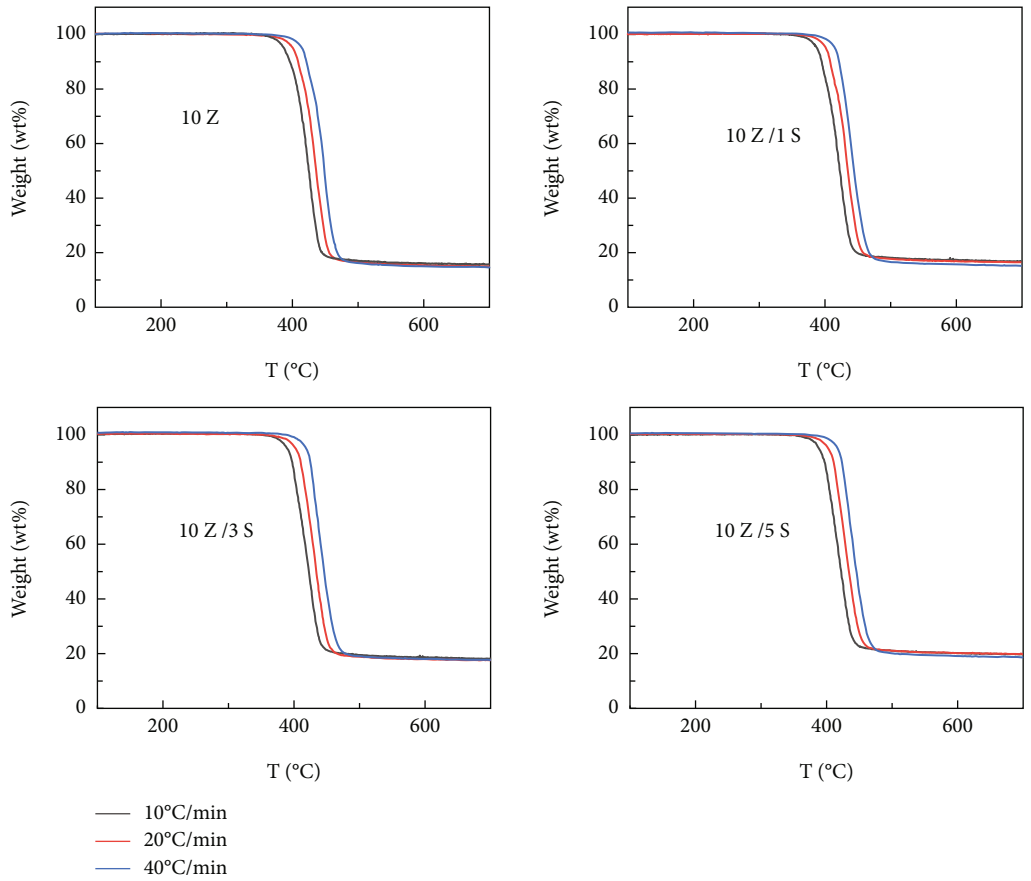

Figure 4: Thermogravimetric curve under different heating rates.

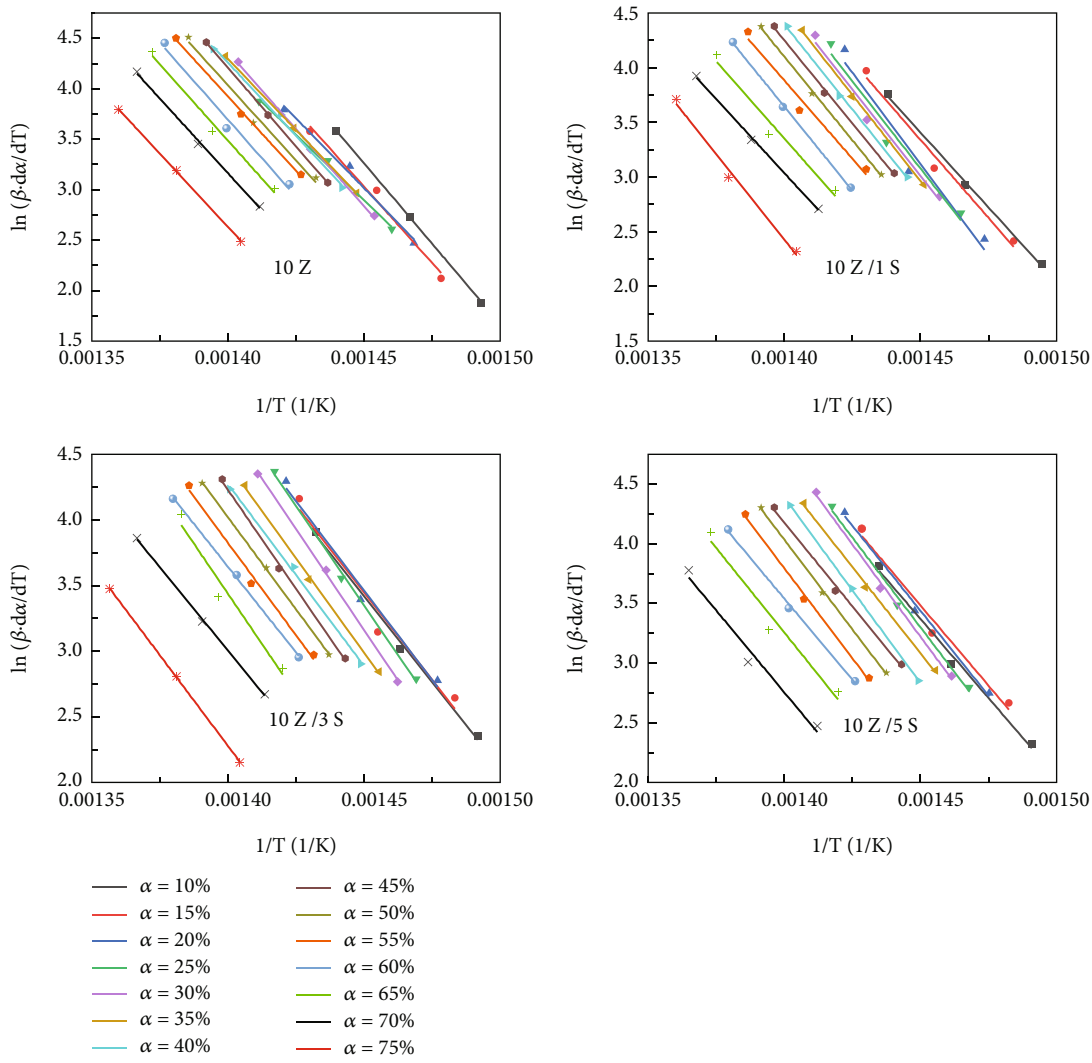

Figure 5: Isoconversional methods applied to TG data of various samples at different heating rates in nitrogen.

which is independent of temperature in the kinetic calculation of single-step thermal decomposition.

Figure 4 shows the thermogravimetric curves of each sample at different heating rates. Taking into account the "thermal hysteresis effect" caused by high heating rates and the need to minimize errors, three heating rates of 10, 20, and 40°C/min are selected.

According to the calculation and fitting of the differential isoconversional model, the diagram of relationship between $\ln(\beta_i(d\alpha/dT)_{\alpha,i})$ and $1/T_{\alpha,i}$ for different conversion rates is shown in Figure 5. The thermal decomposition activation energy of each sample at different α was calculated through the slope of lines, and the results are listed in Table 5 and Figure 6. Since the highest conversion rate of PET/ZDP/SiO_2 composites is 80-85% and there is a large error when the conversion rate approaches 0 or the maximum conversion rate, the calculation interval of the activation energy is selected in 10%-75%. All the activation energies Eα at different conversion rates have a good fit with R^2 values greater than 0.900. Meanwhile, the difference between the maximum and minimum values of E_α is approximately 20% of the average activation energy $\overline{E_\alpha}$. So the influence of different conversion rate on activation energy is little, and the thermogravimetric process of each sample in a nitrogen atmosphere can be considered a single-step thermal decomposition process [28].

It can be found that the change trend of average activation energy is the same as that of LOI compared $\overline{E_\alpha}$ of samples. This is because nano-SiO_2 can improve the thermal stability of PET, so the $\overline{E_\alpha}$ has risen from 245KJ/mol to 251KJ/mol after adding 1 wt% nano-SiO_2. However, higher nano-SiO_2 addition will cause agglomeration, which will lead to the occurrence of the "wick effect" and reduce the thermal stability of PET/ZDP/SiO_2 composites. With the increase of nano-SiO_2, its influence on the thermal stability of PET is greater than the "wick effect", so the average activation energy $\overline{E_\alpha}$ improves again.

3.1.4. Micromorphology of Carbon Layer. Micrographs of the carbon layer on the sample surface after the limiting oxygen index test were observed with a scanning electron microscope,

Table 5: Activation energy of various products during thermal decomposition calculated by isoconversional method.

α/%	10Z			10Z/1S			10Z/3S			10Z/5S		
	E_α (KJ/mol)	R^2	P (%)	E_α (KJ/mol)	R^2	P (%)	E_α (KJ/mol)	R^2	P (%)	E_α (KJ/mol)	R^2	P (%)
10	265	0.99	7.9	228	0.99	-9.0	218	0.99	-6.8	221	0.98	-7.9
15	251	0.97	2.3	238	0.96	-5.2	221	0.93	-5.4	224	0.96	-6.5
20	230	0.98	-6.3	278	0.90	10	227	0.97	-3.1	237	0.99	-1.0
25	215	0.99	-12	265	0.93	5.8	252	0.99	7.9	250	0.98	4.4
30	254	0.99	3.6	263	0.96	4.7	256	0.99	9.6	257	0.99	7.4
35	234	0.99	-4.6	262	0.99	4.5	239	0.99	2.3	241	0.99	0.4
40	241	0.99	-1.7	259	0.99	3.3	230	0.99	-1.5	259	0.99	8.3
45	259	0.99	5.7	253	0.99	0.7	251	0.99	7.2	234	0.99	-2.5
50	247	0.97	0.8	254	0.99	1.4	233	0.99	-0.2	250	0.99	4.4
55	245	0.99	-0.2	238	0.95	-5.2	234	0.98	0.1	251	0.99	4.7
60	254	0.97	3.5	255	0.99	1.7	217	0.99	-7.1	227	0.99	-5.4
65	251	0.98	2.3	234	0.94	-6.6	254	0.92	8.6	236	0.93	-1.6
70	246	0.99	0.2	225	0.99	-10	211	0.99	-9.8	228	0.95	-4.7
75	242	0.99	-1.5	260	0.98	3.6	230	0.99	-1.7	—	—	—
$\overline{E\alpha}$	245			251			234			240		

"P" represents the percentage error between the activation energy and the average activation energy.

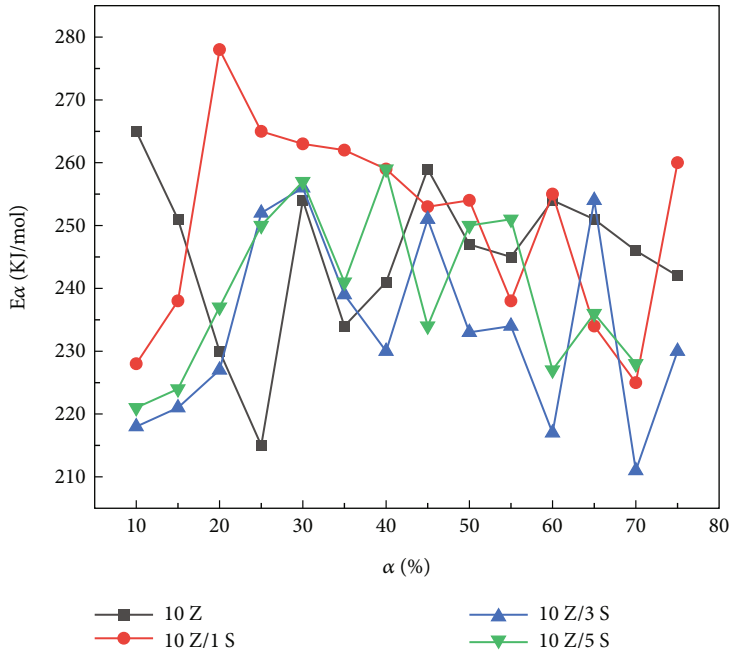

Figure 6: Activation energy of each samples vs. conversion rate.

as shown in Figure 7. It can be seen from SEM images that there were many cracks on the surface of 10Z/1S, and some of them had large holes. Cracks on the carbon layer of 10Z/3S had disappeared, but there were still many small holes. When the nano-SiO_2 content reached 5 wt%, the pores on the carbon layer completely disappeared, and the surface of the carbon layer bulged. The surface of the carbon layer was smooth and dense with a high load of nano-SiO_2 and covered with white particles. This was because nano-SiO_2 would not volatilize and migrate to the char during the combustion of the PET matrix, which would fill into the char. In addition, nano-SiO_2 was easy to form silicon phosphate with phosphoric acid [22, 29], which would fix the carbon layer and improve its thermal stability. A stable carbon layer could effectively isolate the heat generated by combustion from being transferred to the PET matrix. The dense carbon layer formed by nano-SiO_2 could also prevent the mass transfer process inside and outside the carbon layer. With a high load of nano-SiO_2, the combustible gas was completely isolated from overflowing into fire, and the charred layer had swollen.

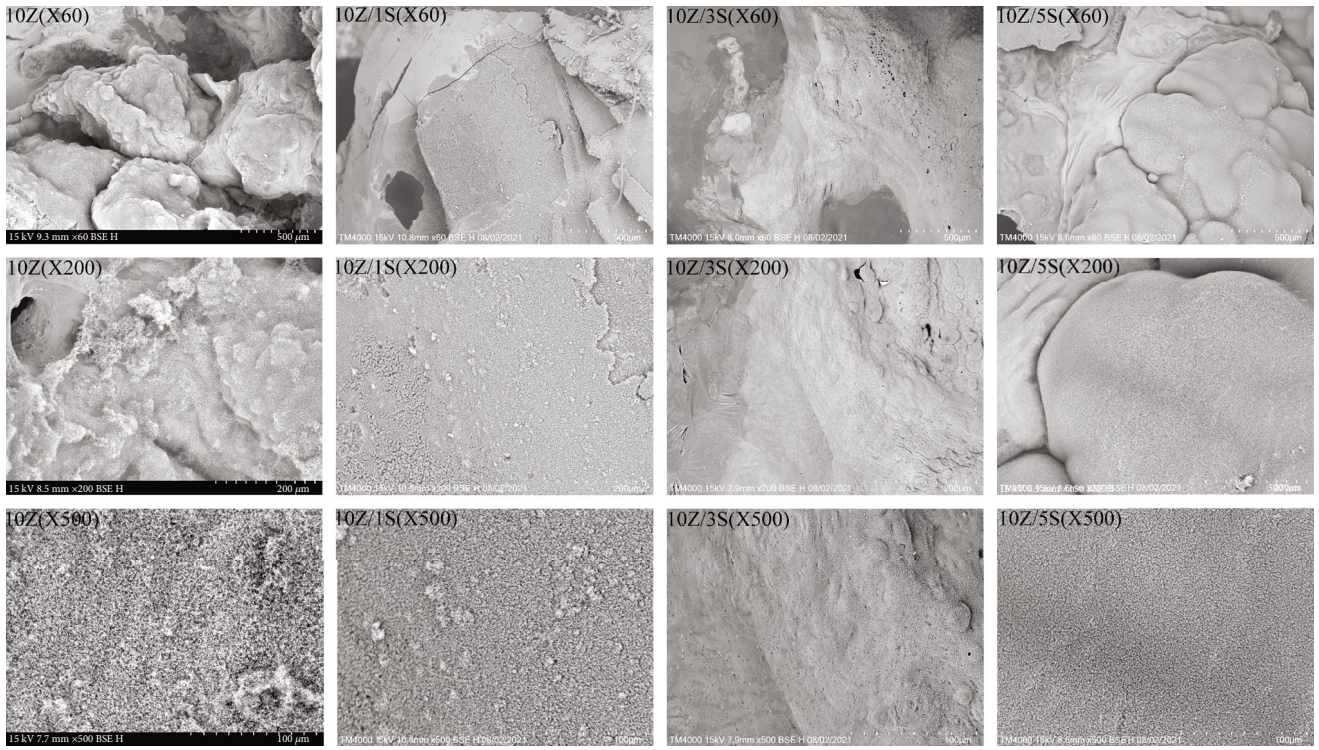

Figure 7: SEM of carbon layer after limiting oxygen index test.

3.2. Foaming Performance and Analysis

3.2.1. Rheological Property. The rheological properties of polymer have a great impact on the foaming process. Most commercial PET has a linear molecular chain with a narrow molecular weight distribution and low-melt viscoelasticity, which is not suitable for foaming. There are many methods to improve the viscoelasticity of PET. Melting reaction with a multifunctional chain extender is a practical method that introduces long-branched chains and/or controllable cross-linking. The long-chain branched structure can greatly improve foamability because it makes the tensile viscosity of the material rise sharply (strain hardening)[30], which plays an important role in the fixation of cell structure after cell growth during the foaming process.

In order to improve the foamability of samples, PMDA was introduced to act as a chain extender. The effect of nano-SiO_2 and ZDP on PET chain extension was examined by using an internal mixer at 270°C and 60 rpm. Figure 8 shows the torque curves of samples over time. A sharp drop in the torque curve was observed, meaning that PET pellets were completely melted at 0~30 sec. After melting, the torque continued to decrease slowly, suggesting that the viscosity was reduced. It was attributed to the increase in melt temperature and thermomechanical degradation. With time increasing, the torque increased due to chain extension/branching reactions. The time for torque to reach a maximum value for 10Z was shorter than that of samples with nano-SiO_2. With an increase of nano-SiO_2 content, the maximum torque gradually decreased, showing that nano-SiO_2 would inhibit the chain extension reaction of PET.

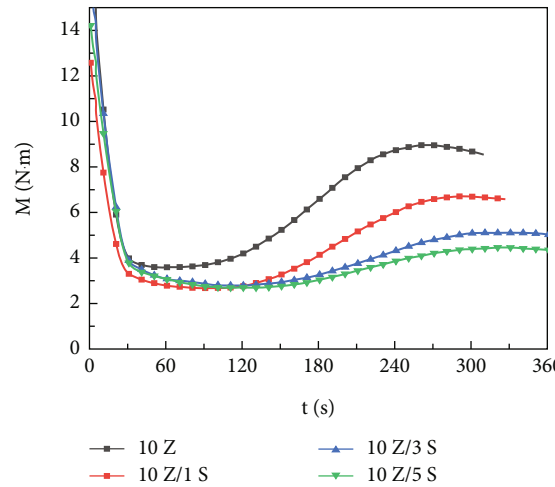

Figure 8: Torque as a function of processing time in the internal mixer.

The rheological properties of each sample are shown in Figure 9. The complex viscosity $|\eta *|$ decreased with the addition of nano-SiO_2. According to research by Ebadi-Dehaghan [31] and Yao [32], nano-SiO_2 improved the modulus and viscosity of PET/SiO_2 nanocomposites by microcrosslinking PET molecular chains. In this paper, the reduction of complex viscosity and storage modulus would be related to the chain extension reaction of PET. Combined with Figure 8, it was believed that the addition of nano-SiO_2 hindered the chain extension reaction of PET. The storage modulus G' tended to have the same value at high frequency, while the absolute

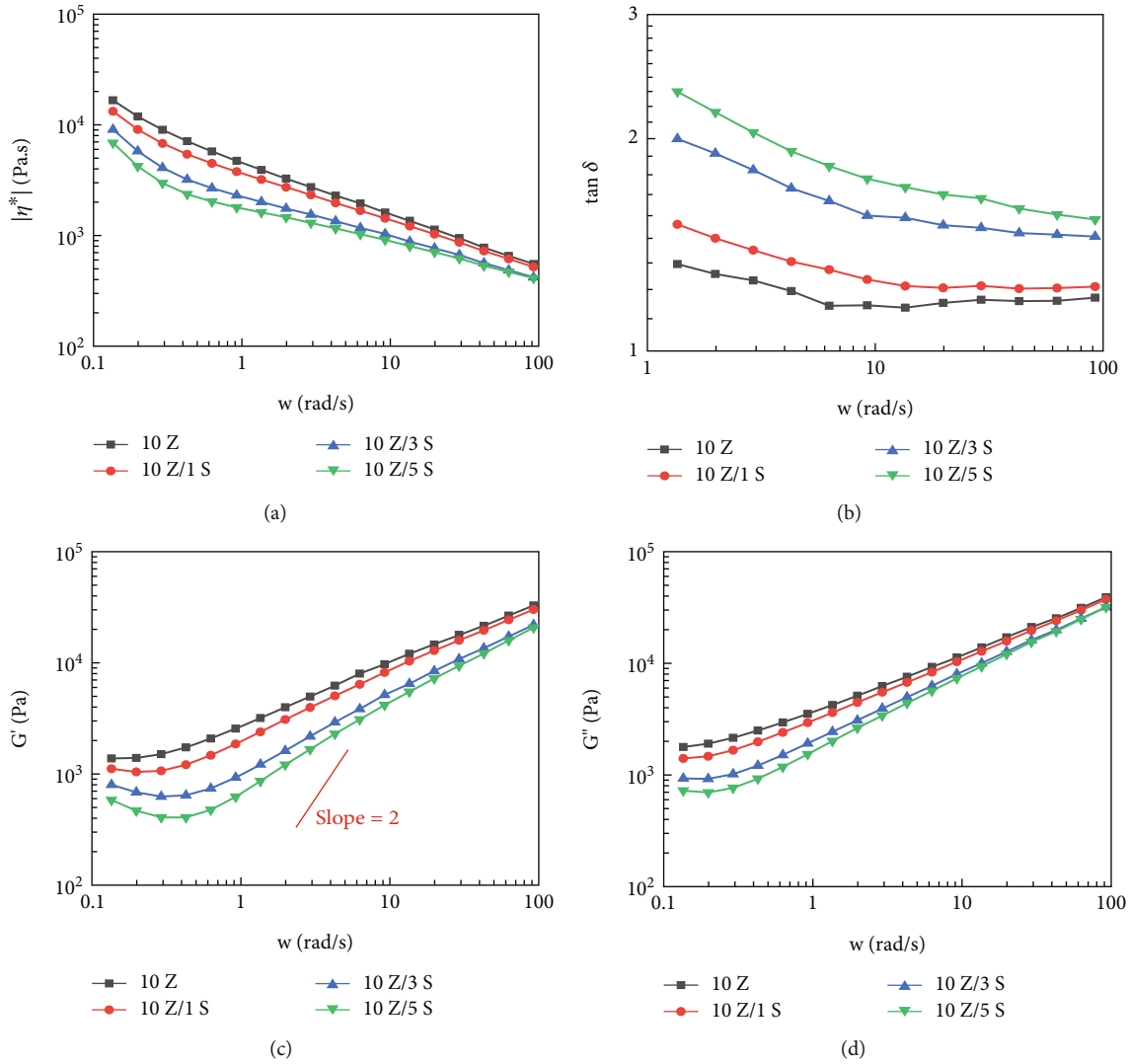

FIGURE 9: Effect of nano-SIO_2 content on rheological properties of pet when zdp content is 10wt%. (a) Complex viscosity $|\eta *|$. (b) Storage modulus G' (c) Loss modulus G''.. (d) Loss tangent tanδ.

value at low frequency began to differ. The storage modulus of linear molecules at a low frequency has the following relationship with angular frequency: $\lg G' \propto 2\lg w$. It could be seen from Figure 9(c) that the slope of the storage modulus and angular frequency of each sample were obviously less than 2, which meant that the chain extender made PET undergo a branching reaction. The slope increased slightly with the addition of nano-SiO_2 content, showing that the branching degree of PET decreased.

The addition of nano-SiO_2 resulted in an obvious increase in loss tangent tanδ. According to the relationship between foaming factor F and loss angle summarized by Park: $F = \rho_f D(\tan\delta)^{0.75} \leq 1.8$, where "$\rho_f$" is the bulk density of foam, and "D" is the average diameter of the cell. It was found that the addition of nano-SiO_2 with a content of more than 1 wt% had a damaging effect on the foaming property of ZDP flame retardant PET.

In order to further analyze the influence of nano-SiO_2 on the molecular topology of PET after chain extension and branching, Cole-Cole diagrams and VGP curves were drawn to characterize the branching structure of each sample, as shown in Figures 10 and 11.

Typical linear molecular chains appeared as complete semicircles in the Cole-Cole diagram. The larger the radius of the circle, the greater the molecular weight. The Cole-Cole curves of each sample in Figure 10 were upturned, showing an incomplete arc. These phenomena indicated that PET had long branched chains after reactive branching. Due to the inhibition of nano-SiO_2 on PET chain extension branching, the radius of the curves reduced, indicating that the molecular weight and number of branched chains decreased.

The VGP curve was first proposed by Van and Palmen [33] in order to verify the practicality of the time-temperature equivalence principle. Then Trinke et al. [34] found that the shape of the VGP diagram of a polymer with a known structure was not affected by the shape of the polymer, but it was related to the branched structure of the

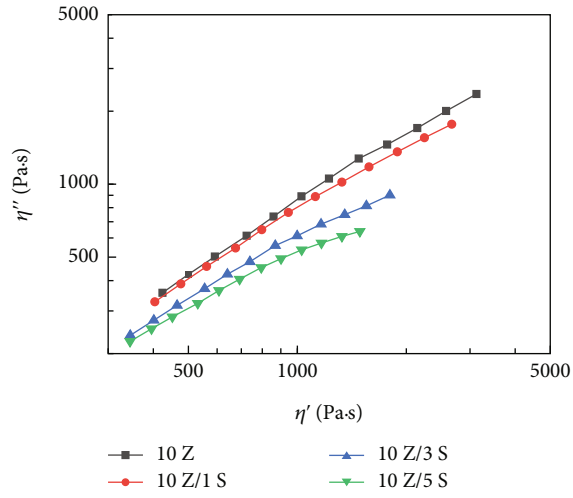

Figure 10: Cole-Cole curve.

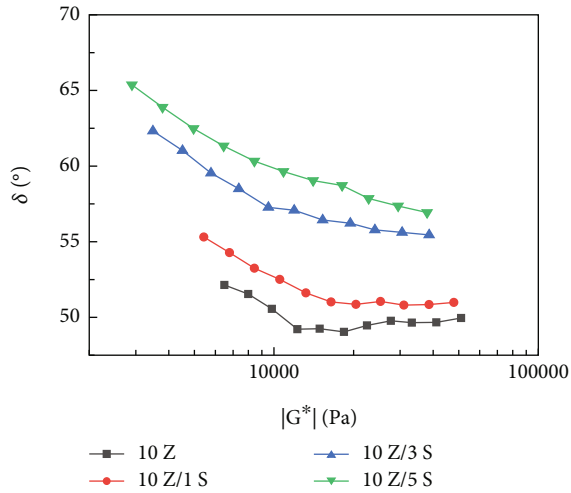

Figure 11: VGP curve.

polymer, which was used to qualitatively judge the molecular topology of an unknown polymer. The VGP curve of linear PET was obviously convex. As the complex modulus decreased, the loss angle increased continuously. A platform close to 90° was finally formed in the region of low complex modulus. However, all curves in Figure 11 were concave to varying degrees. They constantly approached the angle of high modulus and low loss with a reduction of nano-SiO_2 content, which also confirmed the branched structure in the PET molecular chain. Particularly, there was an obvious downward inflection point in the curve, which could be seen in the curves of 10Z and 10Z/1S. This point indicated that the branching degree of the PET molecular chain was higher at low nano-SiO_2 content.

According to the viscoelastic foaming window for PET foaming proposed by Yang [35], although nano-SiO_2 inhibited crosslinking and branching of PET, all samples were still in the foaming window at some temperatures. In summary, the four samples still had good foaming properties.

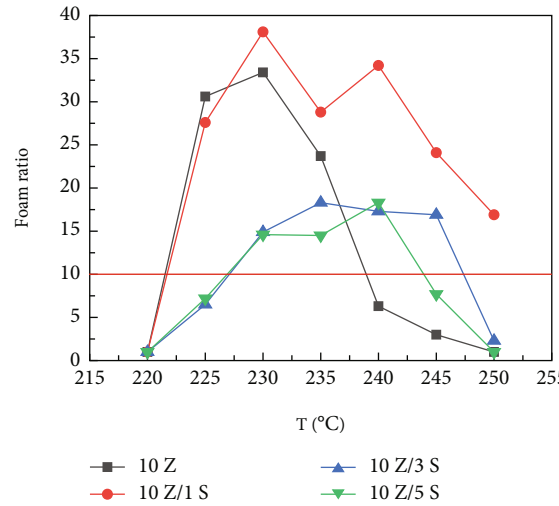

Figure 12: Foaming ratio of ZDP flame retardant pet with different content of nano-sio_2 synergistic effect (above the red line represents the appropriate foaming ratio).

Table 6: Foaming ratio of samples at various foaming temperature.

Temperature/°C	220	225	230	235	240	245	250
10Z	1	30. 6	33. 4	23. 7	6. 3	3	1
10Z/1S	1	27. 6	38. 1	28. 8	34. 2	24. 1	16. 9
10Z/3S	1	6. 5	14. 9	18. 3	17. 3	16. 9	2. 3
10Z/5S	1	7. 2	14. 6	14. 5	18. 3	7. 7	1

3.2.2. Foaming Properties of Nano-SiO2 Synergistic ZDP Flame Retardant PET. Figure 12 and Table 6 show the foaming ratios of the foaming products of each sample. For sample 10Z, its foaming ratio was more than 20 times within the appropriate foaming temperature range of 225-235°C. The expansion ratio of 10Z/1S was larger than that of 10Z, and the foaming temperature zone was extended to a higher temperature. Although the suitable foaming temperature zone was still wider than 10Z, the foaming ratio rapidly reduced if the content of nano-SiO_2 continued to increase. The maximum foaming ratio of 10Z/3S and 10Z/5S samples failed to reach 20 times. Particularly, it was found that the appropriate temperature zone shifted to a higher temperature zone with the addition of nano-SiO_2.

The influence of temperature on the foaming performance of each sample was similar. The foaming ratios firstly raised and then reduced with the increase in temperature. This phenomenon was attributed to the fact that temperature affected two important parameters of foaming at the same time: melt strength and CO_2 solubility. PET had higher melt strength and viscoelasticity at low temperature, which greatly limited the growth of cells. The melt strength and viscoelasticity of PET decreased with the increase in temperature, which made the cell to grow easily, resulting in a rise in foaming ratio. However, when the temperature was high, the solubility of CO_2 would decrease. The reduction can decrease the power source of cell nucleation and slow the growth of cells. As a result, the strength of PET melt was

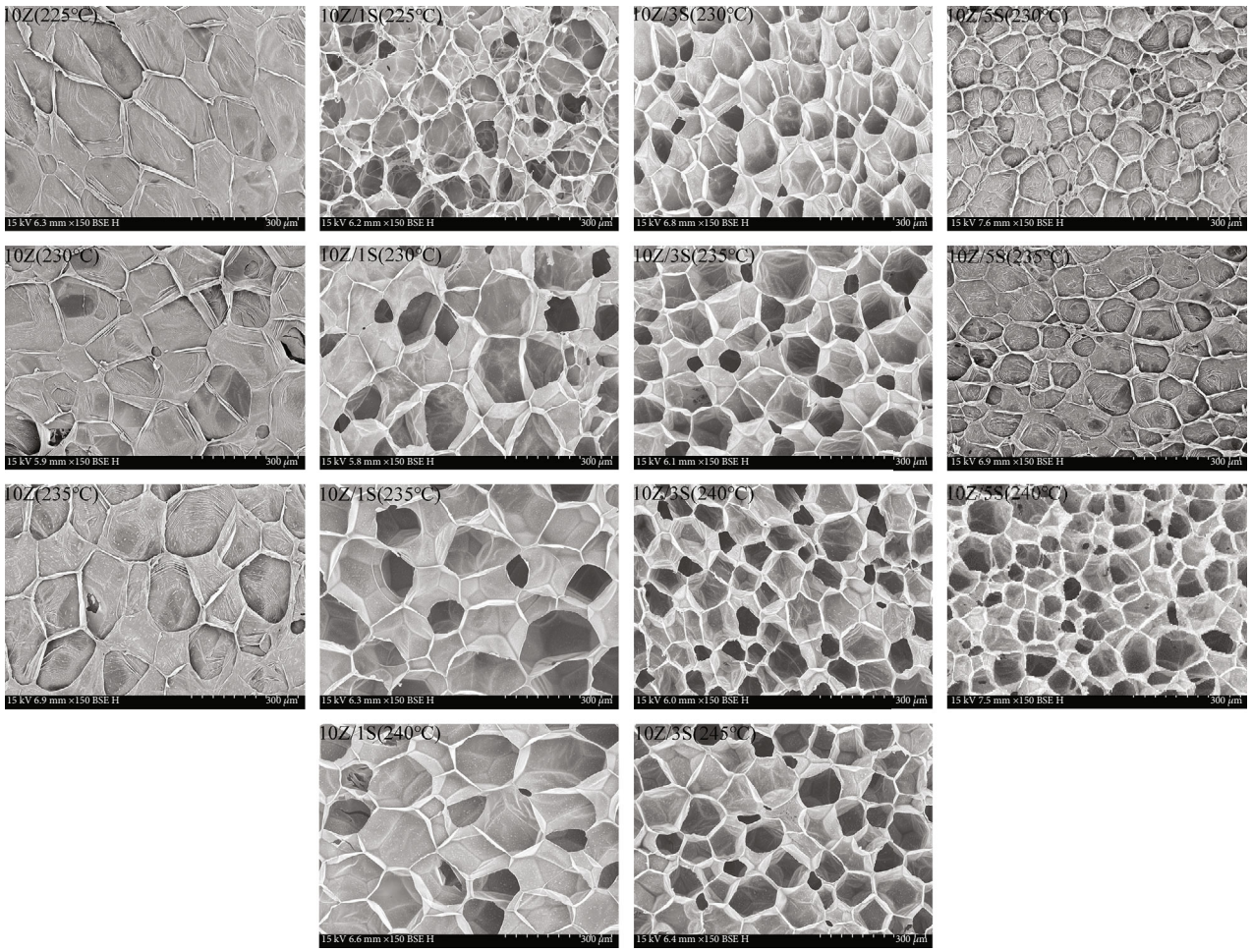

Figure 13: SEM of cell structure (x150).

too low to support cell growth, resulting in cell fracture and consolidation, which led to a reduction in the foaming ratio. In addition, the foaming ratio of all samples suddenly decreased and failed to be foam at 220°C.

The cell structure was observed by scanning electron microscopy, and the cell diameter and cell density of each foaming sample were counted by ImageJ software, as shown in Figures 13–15. The cells had a typical closed structure, and the through-hole phenomenon increased with the addition of temperature. Nano-SiO_2 had a great influence on cell density and cell structure. The cell diameter decreased, and the cell density increased with the addition of nano-SiO_2 content, but the degree of cell irregularity rose. According to the analysis of cell structure, the increase in the foaming ratio was a result of the addition of cell density when adding 1 wt% nano-SiO_2. While the reduction of foaming ratio under higher nano-SiO_2 content was due to the decrease in cell diameter.

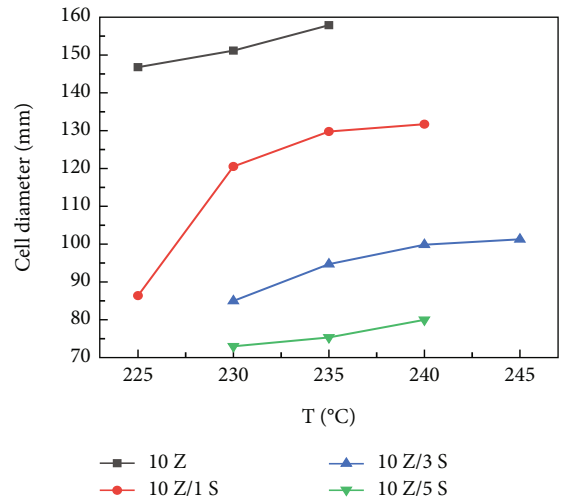

Figure 14: Cell diameter.

3.2.3. Thermal Properties and their Influence on Cellular Structure. Crystallization behavior of PET is an important parameter that affects the cellular structure of PET. The low potential energy in the crystalline and amorphous regions is conducive to cell nucleation. Crystallization greatly increases the melt strength of PET and affects the size of the cell diameter. However, an excessive crystallization area will hinder the growth of the cell and change its shape. Crystallization also reduces the solubility of CO_2 in PET, thereby affecting the cellular structure. Therefore, changes

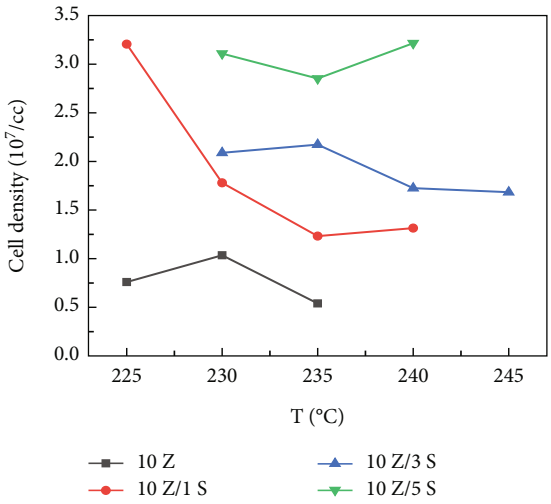

Figure 15: Cell density.

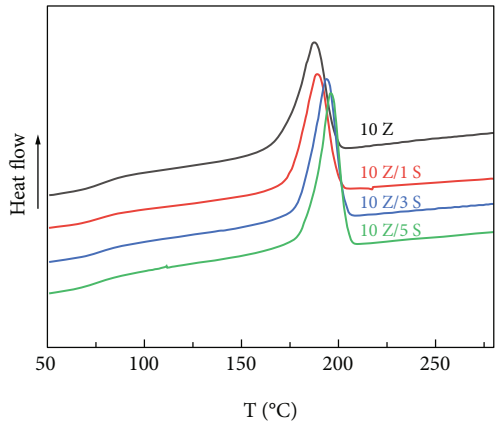

Figure 16: Cooling curve.

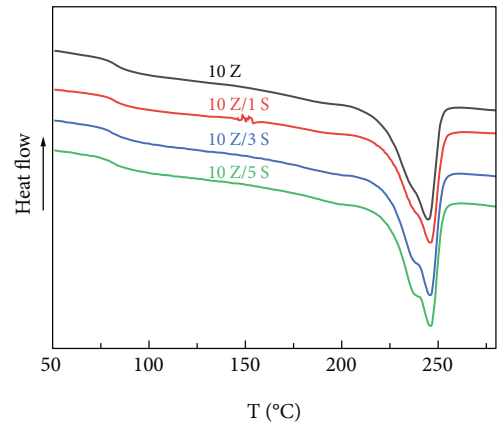

Figure 17: Temperature rise curve.

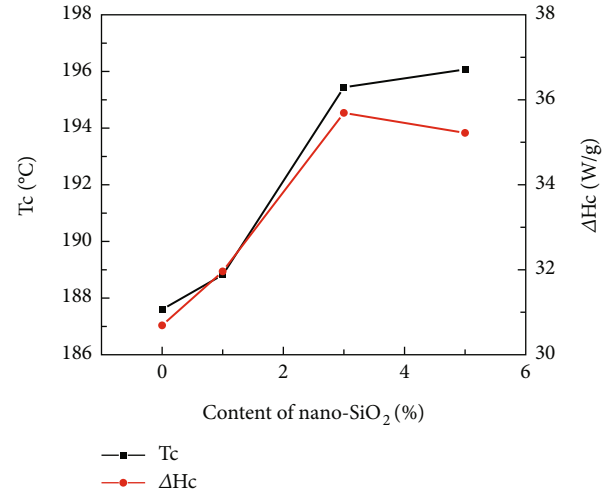

Figure 18: Relationship between crystallization temperature, crystallization enthalpy, and nano-SIO_2 content.

in cell structure can be analyzed through the thermal properties of PET.

The heating and cooling curves of each sample are shown in Figures 16 and 17. Figure 18 shows the crystallization temperature (Tc) and crystallization enthalpy (H_c). Tc and H_c increase with the addition of nano-SiO_2 content. Especially for the 10Z/3S and 10Z/5S samples, T_c has risen by more than 7°C compared to 10Z/1S. Besides, the addition of nano-SiO_2 also narrows the crystallization peak, indicating the crystallization rate increases. This is because nano-SiO_2 acts as a nucleating agent, which can promote the crystallization of PET. Nano-SiO_2 and ZDP also inhibit the chain extension and branching of PET molecules, resulting in a reduction of molecular weight and branching degree of PET. The reduction makes the molecular chain of PET easier to arrange in an orderly when cooling.

According to the classical nucleation theory [36], the nucleation barrier at the interface between crystalline and amorphous regions of PET is lower, which is beneficial to cell nucleation. The addition of nano-SiO_2 greatly improves the crystallization ability of PET, resulting in a rise in cell density with an increase in nano-SiO_2 content. It also reduces melt strength of PET/ZDP composites, so the cell diameter increases. The foaming ratio reduces the load of nano-SiO_2 over 3 wt%. The reason is that crystallization can reduce thesolubility of CO_2, and the crystal region can inhibit the growth of cell, which is also the cause of irregular cell structure. When the content is 1 wt%, the benefit of cell nucleation is greater than its effect on the decrease of CO_2 solubility. The inhibition of crystal region on cell growth is low, so the foaming ratio increases. Additionally, crystallization can increase melt strength, which prevents the cell wall from breaking during growth process. Therefore, the foaming temperature range and the optimal foaming temperature increased after adding nano-SiO_2.

4. Conclusion

The synergistic effect of nano-SiO_2 and ZDP on the flame-retardant properties of PET was studied, and the effect of nano-SiO_2 on the foaming properties of PET/ZDP composites was analyzed. When 10 wt% ZDP was introduced into PET, the limiting oxygen index increased to 28.5%, but UL-94 only reached grade V-2 due to its failure to inhibit

the generation of dripping. After adding 5 wt% nano-SiO_2, the dripping phenomenon was inhibited owing to the stability of the carbon layer and the increase in surface quality.

Both ZDP and nano-SiO_2 had an inhibitory effect on chain extension and branching, which reduced the viscoelasticity of PET. However, when the ZDP content was 10 wt% and the nano-SiO_2 content was lower than 5 wt%, PET still had good foam performance. Its not only widened the foaming temperature range of PET but also increased the foaming ratio by increasing the cell density with a 1 wt% the content of nano-SiO_2. While the load reached 5 wt%, the foaming ratio dropped to about 15 times, which still met requirements of industrialized PET foam materials.

In summary, the combination of ZDP and nano-SiO_2 reduced the impact of flame retardant on the viscoelasticity of PET melt through the good compatibility between ZDP and PET. At the same time, SiO_2 not only improved the fire resistance of PET by making the carbon layer compact but also improved the foaming performance of flame-retardant PET by increasing the crystallization performance of PET. However, the foaming ratio will decrease with a high load of SiO_2, which requires other solutions to obtain lighter PET flame-retardant foaming materials.

Data Availability

The data used to support the findings of this study are included within the article.

Conflicts of Interest

The authors declare that they have no conflicts of interest.

References

[1] C.-C. Lai, C.-T. Yu, F.-M. Wang et al., "Preparation of recycled polyethylene terephthalate composite foams and their feasible evaluation for electronic packages," *Polymer Testing*, vol. 74, pp. 1–6, 2019.

[2] G. Lu, W. D. van Driel, X. Fan et al., "Degradation of microcellular PET reflective materials used in LED-based products," *Optical Materials*, vol. 49, pp. 79–84, 2015.

[3] W.-B. Liu, Y.-X. Liu, Z. Yang, Q. Wu, and N.-C. Wang, "Application and popularization prospect of PET core material in wind turbine blades," *Tianjin Science & Technology*, vol. 48, pp. 66-67, 2021.

[4] N. Didane, S. Giraud, E. Devaux, and G. Lemort, "A comparative study of POSS as synergists with zinc phosphinates for PET fire retardancy," *Polymer Degradation and Stability*, vol. 97, no. 3, pp. 383–391, 2012.

[5] H. B. Zhao and Y. Z. Wang, "Design and synthesis of PET-based copolyesters with flame-retardant and antidripping performance," *Macromolecular Rapid Communications*, vol. 38, no. 23, 2017.

[6] M. Kilinc, G. O. Cakal, G. Bayram, I. Eroglu, and S. Özkar, "Flame retardancy and mechanical properties of pet-based composites containing phosphorus and boron-based additives," *Journal of Applied Polymer Science*, vol. 132, no. 22, 2015.

[7] Y. Zhang, L. Chen, J.-J. Zhao et al., "A phosphorus-containing PET ionomer: from ionic aggregates to flame retardance and restricted melt-dripping," *Polymer Chemistry*, vol. 5, no. 6, pp. 1982–1991, 2014.

[8] X. Ao, Y. Du, D. Yu et al., "Synthesis, characterization of a DOPO-based polymeric flame retardant and its application in polyethylene terephthalate," *Progress in Natural Science: Materials International*, vol. 30, no. 2, pp. 200–207, 2020.

[9] Z.-H. Peng, C.-X. Guo, Z.-H. Peng, L.-Y. Tong, W.-Q. Peng, and C.-S. Wang, "Flame retardant polyester fiber and its preparation method[P]," 2020, Chinese Patent: CN110923841A.

[10] Y. Cheng, Y. Wang, F. He et al., "Kinetics and properties of phosphorus flame retardant copolymerized polyester," *Journal of Textile Research*, vol. 40, pp. 10–13, 2019.

[11] L. Gao, Y.-K. Ge, Z.-M. Xu, T. Liu, and L. Zhao, "Development of ZDP/nano-Al2O3 flame retardant modified PET extrusion foaming material," *Engineering Plastics Application*, vol. 47, pp. 7–14, 2019.

[12] A. Dasari, Z.-Z. Yu, G.-P. Cai, and Y.-W. Mai, "Recent developments in the fire retardancy of polymeric materials," *Progress in Polymer Science*, vol. 38, no. 9, pp. 1357–1387, 2013.

[13] X. Zhou, S. Qiu, X. Mu et al., "Polyphosphazenes-based flame retardants: A review," *Composites Part B: Engineering*, vol. 202, article 108397, 2020.

[14] M. Lewin and E. D. Weil, "Mechanisms and modes of action in flame retardancy of polymers," *Fire Retardant Materials*, vol. 1, pp. 31–68, 2001.

[15] M. Doğan, S. Erdoğan, and E. Bayramlı, "Mechanical, thermal, and fire retardant properties of poly(ethylene terephthalate) fiber containing zinc phosphinate and organo-modified clay," *Journal of Thermal Analysis and Calorimetry*, vol. 112, no. 2, pp. 871–876, 2013.

[16] F. Salaün, G. Lemort, C. Butstraen, E. Devaux, and G. Capon, "Influence of silica nanoparticles combined with zinc phosphinate on flame retardant properties of PET," *Polymers for Advanced Technologies*, vol. 28, no. 12, pp. 1919–1928, 2017.

[17] N. Mandlekar, G. Malucelli, A. Cayla et al., "Fire retardant action of zinc phosphinate and polyamide 11 blend containing lignin as a carbon source," *Polymer Degradation and Stability*, vol. 153, pp. 63–74, 2018.

[18] G. Beyer, "Nanocomposites offer new way forward for flame retardants," *Additives and Compounding*, vol. 7, no. 5, pp. 32–35, 2005.

[19] T. Kashiwagi, F. Du, J. F. Douglas, K. I. Winey, R. H. Harris Jr., and J. R. Shields, "Nanoparticle networks reduce the flammability of polymer nanocomposites," *Nature Materials*, vol. 4, no. 12, pp. 928–933, 2005.

[20] D.-Y. Wang, Y.-Z. Wang, J.-S. Wang et al., "Thermal oxidative degradation behaviours of flame-retardant copolyesters containing phosphorous linked pendent group/montmorillonite nanocomposites," *Polymer Degradation and Stability*, vol. 87, no. 1, pp. 171–176, 2005.

[21] J. Zheng, P. Cui, X. Tian, and K. Zheng, "Pyrolysis studies of polyethylene terephthalate/silica nanocomposites," *Journal of Applied Polymer Science*, vol. 104, no. 1, pp. 9–14, 2007.

[22] M. Gao, W. Wu, and Z. Q. Xu, "Thermal degradation behaviors and flame retardancy of epoxy resins with novel silicon-containing flame retardant," *Journal of Applied Polymer Science*, vol. 127, no. 3, pp. 1842–1847, 2013.

[23] J. Xu, *Study on the Preparetion and Properties of PS Microcellular Foam*, Shangdong University, 2018.

[24] F. Yang and G. L. Nelson, "PMMA/silica nanocomposite studies: synthesis and properties," *Journal of Applied Polymer Science*, vol. 91, no. 6, pp. 3844–3850, 2004.

[25] B.-P. Yang, B.-B. Chen, J.-F. Cui et al., "Preparation and flammability property of flame retardant polyester/SiO_2 nanocomposite," *Engineering Plastics Application*, vol. 42, pp. 9–14, 2014.

[26] I. van der Veen and J. de Boer, "Phosphorus flame retardants: properties, production, environmental occurrence, toxicity and analysis," *Chemosphere*, vol. 88, no. 10, pp. 1119–1153, 2012.

[27] S. Vyazovkin, A. K. Burnham, J. M. Criado, L. A. Pérez-Maqueda, C. Popescu, and N. Sbirrazzuoli, "ICTAC kinetics committee recommendations for performing kinetic computations on thermal analysis data," *Thermochimica Acta*, vol. 520, no. 1-2, pp. 1–19, 2011.

[28] S. Vyazovkin, A. K. Burnham, L. Favergeon et al., "ICTAC Kinetics Committee recommendations for analysis of multi-step kinetics," *Thermochimica Acta*, vol. 689, article 178597, 2020.

[29] Q. He, L. Song, Y. Hu, and S. Zhou, "Synergistic effects of polyhedral oligomeric silsesquioxane (POSS) and oligomeric bisphenyl A bis(diphenyl phosphate) (BDP) on thermal and flame retardant properties of polycarbonate," *Journal of Materials Science*, vol. 44, no. 5, pp. 1308–1316, 2009.

[30] D. J. Lohse, S. T. Milner, L. J. Fetters et al., "Well-defined, model long chain branched polyethylene. 2. melt rheological behavior," *Macromolecules*, vol. 35, no. 8, pp. 3066–3075, 2002.

[31] H. Ebadi-Dehaghani, P. Hassanzadeh, and K. Ansari, "The ability of rheological studies for assessment of hydrolysis during processing of polyethylene terephthalate nanocomposites," *Journal of Macromolecular Science, Part B*, vol. 53, no. 11, pp. 1750–1762, 2014.

[32] X. Yao, X. Tian, D. Xie et al., "Interface structure of poly(ethylene terephthalate)/silica nanocomposites," *Polymer*, vol. 50, no. 5, pp. 1251–1256, 2009.

[33] M. Van Gurp and J. Palmen, "Time-temperature superposition for polymeric blends," *Rheology Bulletin*, vol. 67, pp. 5–8, 1998.

[34] S. Trinkle, P. Walter, and C. Friedrich, "Van Gurp-Palmen plot II–classification of long chain branched polymers by their topology," *Rheologica Acta*, vol. 41, pp. 103–113, 2002.

[35] Z.-P. Yang, *Study on Rheological Properties of High-Expansion-Ratio Pet Resin and Regulating Mechanism of Foam Structure*, Beijing University of Chemical and Technology, 2017.

[36] J. S. Colton and N. P. Suh, "Nucleation of microcellular foam: theory and practice," *Polymer Engineering & Science*, vol. 27, no. 7, pp. 500–503, 1987.